31st Annual International Conference of the IEEE EMBS
Minneapolis, Minnesota, USA, September 2-6, 2009

Unsupervised Segmentation of the Prostate Using MR Images Based on Level Set with a Shape Prior

Xin Liu, D. L. Langer, M. A. Haider, T. H. Van der Kwast, A. J. Evans, M. N. Wernick, and I. S. Yetik

***Abstract*—Prostate cancer is the second leading cause of cancer death in American men. Current prostate MRI can benefit from automated tumor localization to help guide biopsy, radiotherapy and surgical planning. An important step of automated prostate cancer localization is the segmentation of the prostate. In this paper, we propose a fully automatic method for the segmentation of the prostate. We firstly apply a deformable ellipse model to find an ellipse that best fits the prostate shape. Then, this ellipse is used to initiate the level set and constrain the level set evolution with a shape penalty term. Finally, certain post processing methods are applied to refine the prostate boundaries. We apply the proposed method to real diffusion-weighted (DWI) MRI images data to test the performance. Our results show that accurate segmentation can be obtained with the proposed method compared to human readers.**

***Index Terms*—Image segmentation, prostate, magnetic resonance imaging, level set, shape prior**

I. Introduction

Prostate cancer is one of the most frequently diagnosed cancer and one of the leading causes of cancer death in American men [1]. Therefore, there is an interest in significant improvements in prostate cancer diagnosis and treatment. Imaging methods that could provide reliable information about the size and shape of prostate gland and localize the cancer foci would improve the accuracy of diagnosis and enable more efficient treatment. Currently, the most widely-used modality for prostate cancer diagnosis is trans-rectal ultrasound (TRUS) because of its low cost and short acquisition time. However, its performance of prostate cancer visualization is poor. Recent studies have shown that magnetic resonance imaging (MRI) has higher accuracy in the detection of prostate cancer [2]. Prostate volume is routinely asked as part of imaging evaluation as it helps in clinical decision making when combined with serum prostate specific antigen (PSA) to derive PSA density [3]. Knowledge of prostate boundaries is also useful in planning of conformal radiation therapy. Knowledge of the voxels within the prostate is also useful in strategies for computer aided prostate cancer segmentation. This task is challenging because of the noise in MR images and the anatomical complexity of prostate.

In the literature, a variety of methods have been presented for prostate segmentation. For TRUS images, several methods [4], [5] have been proposed, and different deformable models were applied. In [4], the prostate shape is modeled as deformable superellipses based on a training dataset. In [5], a level set framework fusing TRUS image histogram information is applied. Compared with TRUS images, research in prostate segmentation of MR images is limited. In [6], the shape information obtained by training is introduced in level set deformation. In [7], a semi-automatic method based on flow orientation is applied.

In this paper, we propose an unsupervised method based on level set with a shape prior to segment the prostate from multispectral MR images that does not require training. To deal with the complex prostate anatomy and partially missing boundaries, we assume the shape of prostate is approximately elliptical, and find an ellipse, which fits the prostate region to initiate the level set and to constrain the level set evolution. Then, level set method with a shape prior is applied to obtain the prostate boundary. Finally, we apply some post processing operations to further refine prostate boundaries.

This paper organized as follows. Section II describes the basics of our method. In Section III, the experimental results obtained using our method are illustrated. Conclusions and future work are presented in Section IV.

II. Segmentation Method

The proposed fully automatic segmentation method consists of three main steps: the first step is applying a deformable ellipse model to find the best ellipse that fits the prostate; the second step is find the actual boundary of the prostate by shape-based level set method; the last step is connectivity and morphological analysis as well as gradient-based corrections to refine prostate boundary. Each of these steps is described in detail next.

A. Shape Information Extraction

Medical image segmentation in general faces difficulties including noise, missing boundaries, and complex anatomical structures. Under such conditions, introducing some prior information, such as the general shape, location, intensity, and curvature profile of the tissue of interest could help the segmentation algorithm perform better. In MR images, the prostate and surrounding tissues have overlapping intensity and texture, and prostate boundaries may be missing, or

This work is partially supported by prostate cancer research foundation of Canada.

Xin Liu, M. N. Wernick, and I. S. Yetik are with Medical Imaging Research Center, Illinois Institute of Technology, Chicago, IL.

D. L. Langer and M. A. Haider are with Institute of Medical Science, University of Toronto, Ontario, and Joint Department of Medical Imaging, Princess Margaret Hospital, University Health Network and Mount Sinai Hospital, Ontario.

T. H. Van der Kwast is with Department of Surgical Oncology, Princess Margaret Hospital, University Health Network, Ontario.

A. J. Evans is with Department of Pathology and Laboratory Medicine, Toronto General Hospital, University Health Network, Ontario.

blended with surrounding tissues. However, generally, the prostate has a walnut-like shape. Combining shape prior information that the prostate is elliptical could constrain the segmentation algorithm and help it extract the prostate automatically.

We first threshold the MR image to obtain a rough prostate region and extract the shape information for further segmentation. We use an optimal thresholding method [8] to select the threshold automatically by Otsu's method. The main idea of Otsu's thresholding is choosing the threshold which minimizes the intra-class variance which is defined as a weighted sum of variances of the two hard classes:

$$\sigma^2_{intra}(T) = q_1(T)\sigma^2_1(T) + q_2(T)\sigma^2_2(T), \tag{1}$$

where $q_1(T)$ and $q_2(T)$ are the probabilities of the two hard classes defined by the threshold T, $\sigma^2_1(T)$ and $\sigma^2_2(T)$ are variances of these two classes. Intra-class variance $\sigma^2_{intra}(T)$ can be calculated for all possible threshold values and the one that minimizes the intra-class variance $\sigma^2_{intra}(T)$ is selected.

After thresholding, we model the prostate shape by a parametric ellipse:

$$\phi(x,y) = 1 - \frac{(x-a_x)^2}{r_x^2} + \frac{(y-a_y)^2}{r_y^2}, \tag{2}$$

where (a_x, a_y) is the center of the ellipse, and r_x,r_y are the lengths of the semi axes. Shape parameters (a_x, a_y, r_x, r_y) completely define an ellipse, and these are the parameters to be estimated as follows. We use a shape comparison cost function as:

$$E_{shape}(\phi, U) = \int_\Omega (H(\phi) - U)^2 dxdy, \tag{3}$$

where Ω is the image domain, ϕ the deformable ellipse, $H(\cdot)$ heaviside function and U the binary image obtained after thresholding. Manually defining the initial estimates of the shape parameter, and minimizing (3) the difference between the binary image and deformable ellipse by gradient descent method, we can obtain a set of (a_x, a_y, r_x, r_y) defining an ellipse, which best fits the prostate. The result of $H(\phi)$ is a binary image, where $H(\phi(x,y)) = 1$ inside of the ellipse, and $H(\phi(x,y)) = 0$ elsewhere.

B. Level Set with Shape Information

Level set method is a numerical technique that can follow the evolution of interfaces. It has been applied to various image processing applications including image segmentation, reconstruction, and denoising. Level set method was firstly introduced in image processing in [9]; Chan and Vese proposed a new model combines the Mumford-Shah's functional and level set method in [10]. Recently, level set based variational approaches that incorporates shape priors are proposed in [11], [12], using different shape models. In [5] and [6], level set method was applied to prostate segmentation for TRUS and MR datasets, respectively. In the previous studies, the shape-based segmentation approaches are either based on the exact shape known a prior [11], [12], or the shape parameters are obtained from training data [4], [6]. In this paper, considering the variety of prostate shapes, the shape information is extracted by a separate unsupervised step from MR image, and introduced to the model as a penalty term to constrain the level set deformation.

In [10], Chan and Vese proposed a variational model based on a level set function ψ, whose zero level set $\psi(x,y) = 0$ segments the image into several intensity homogeneous regions, and the evolution of segmentation is given by the zeros-level curve at time t of the function $\psi(t,x,y)$. The cost function is:

$$\begin{aligned} E_{CV}(\psi, c_1, c_2) &= \int_\Omega (u-c_1)^2 H(\psi) dxdy \\ &\quad + \int_\Omega (u-c_2)^2 (1-H(\psi)) dxdy \\ &\quad + \mu \cdot Length(\psi = 0), \end{aligned} \tag{4}$$

where u is the segmentation image, $H(\cdot)$ the Heaviside function, and c_1, c_2 are the average intensities of the two regions segmented by the zero level set:

$$\begin{aligned} c_1 &= \frac{\int_\Omega u(x,y) H(\psi(x,y)) dxdy}{\int_\Omega H(\psi(x,y)) dxdy}, \\ c_2 &= \frac{\int_\Omega u(x,y)(1 - H(\psi(x,y))) dxdy}{\int_\Omega (1 - H(\psi(x,y))) dxdy}. \end{aligned} \tag{5}$$

The shape difference between the current zero level set: $H(\psi)$ and shape prior ϕ is:

$$E_{shape}(\psi, \phi) = \int_\Omega (H(\psi) - H(\phi))^2 dxdy. \tag{6}$$

Combining (4) and (6), we have our cost function for shape prior based level set:

$$\begin{aligned} E_\psi(\psi, c_1, c_2) &= E_{CV} + E_{shape} \\ &= \int_\Omega (u-c_1)^2 H(\psi) dxdy \\ &\quad + \int_\Omega (u-c_2)^2 (1-H(\psi)) dxdy \\ &\quad + \mu \int_\Omega |\nabla H(\psi)| dxdy \\ &\quad + \beta \int_\Omega (H(\psi) - H(\phi))^2 dxdy, \end{aligned} \tag{7}$$

where μ and β are weighting parameters. Extending (7) to vector images [13], we obtain:

$$\begin{aligned} E_\psi(\psi, c_1, c_2) &= E_{CV} + E_{shape} \\ &= \int_\Omega \frac{1}{N} \sum_{i=1}^{N} (u_i - c_{1i})^2 H(\psi) dxdy \\ &\quad + \int_\Omega \frac{1}{N} \sum_{i=1}^{N} (u_i - c_{2i})^2 (1-H(\psi)) dxdy \\ &\quad + \mu \int_\Omega |\nabla H(\psi)| dxdy \\ &\quad + \beta \int_\Omega (H(\psi) - H(\phi))^2 dxdy, \end{aligned} \tag{8}$$

and for updating the level set function ψ, we have:

$$\frac{\partial \psi}{\partial t} = \delta(\psi)[-\frac{1}{N}\sum_{i=1}^{N}(u_i - c_{1i})^2 + \frac{1}{N}\sum_{i=1}^{N}(u_i - c_{2i})^2 + \mu \cdot div\frac{\nabla\psi}{|\nabla\psi|} + 2\beta(H(\psi) - H(\phi))]. \quad (9)$$

where u_i is the ith channel of the image on Ω, and N is the number of channels.

C. Gradient-Based Improvement

In the MR prostate images, the junction between the prostate and the rectum is very thin with weak contrast, or missing (because they are blended in some cases). In most cases, the level set method without shape prior fails to separate the prostate and rectum. Even the shape information is combined, as we discussed above, certain surrounding tissues are included in the segmented prostate region for some patients. To conquer this difficulty, we applied some post processing methods based on the gradient map to separate the prostate and its surrounding tissues. The gradient map along y direction $G_y(x, y)$ has zero-crossings along the valley between the prostate and surrounding tissues. We define:

$$G_y^+(x, y) = H(G_y(x, y)),$$
$$G_y^-(x, y) = H(-G_y(x, y)). \quad (10)$$

For $G_y^+(x, y)$ shown in Fig. 3(b), there are two components, the upper larger component belongs to the prostate, and the lower smaller component belongs to the rectum. Extracting the lower smaller component in Fig. 3(c) from the segmentation result obtained by level set illustrated in Fig. 3(a), we can see that part of the rectum tissues close to the prostate are removed (as shown in Fig. 3(d)). Then, we apply morphological erosion to Fig. 3(d) and select the largest component which corresponding to the prostate. The result is shown in Fig. 3(e).

After this step, the surrounding tissues included in the prostate region by level set are removed. We apply morphological dilation to restore the boundary and fill the small holes inside the prostate region.

III. EXPERIMENTAL RESULTS

In this paper, the MRI dataset is obtained from patients with biopsy-confirmed prostate cancer. The patients underwent MRI prior to prostatectomy on a 1.5T GE Excite HD platform (GE Medical System, Milwaukee, WI) using a 4-channel phased-array surface coil coupled to an endorectal coil (MEDRAD, Warrendale, PA). For each patient, DWI MRI dataset is acquired with a slice thickness of 3 mm and no gap between slices. Acquisition parameters are: TR/TE=4000/77 ms, 128×256 matrix, ETL=144, BW=166.7 kHz, NEX=10, FOV=14 cm, b=0,600 s/mm^2, phase encode direction left-right. The parameter map ADC is calculated from DWI dataset on a voxel-wise basis.

In our experiment, ADC and DWI images are combined to provide more information about the prostate boundaries and improve the performance of our method.

Patient No.	Pt.1	Pt.2	Pt.3	Pt.4	Pt.5
DSC	0.95	0.94	0.91	0.95	0.93
Patient No.	Pt.6	Pt.7	Pt.8	Pt.9	Pt.10
DSC	0.86	0.86	0.87	0.90	0.94

TABLE I
DISC MEASURE VALUES FOR DIFFERENT PATIENTS' RESULT, AND THE MEAN OF DSC IS 0.91 ± 0.03.

Fig. 1(a) and (b) show the original MR images. Comparing DWI and ADC images, we can see that DWI images have higher contrast between prostate and rectum; however, in most cases, the prostate upper boundary is very weak or partially missed due to shadow areas. ADC images have better contrast for the upper boundaries of the prostate, whereas the junctions between prostate and rectum is very weak. Fig. 2(a) shows the binary image of ADC image after thresholding, (b) the initial deformable ellipse, and (c) the deformable ellipse, which best fits the prostate can roughly model the prostate shape. This ellipse is used to initialize and constrain the level set evolution with a penalty term. Both ADC and DWI images are combined forming a vector image to perform the level set segmentation, because part of the prostate boundaries are missing or weak either in DWI or ADC images. Fig. 2(d) is the segmentation result obtained by shape-based level set, and we define the parameters manually, $\beta = 100$ and $\mu = 0.1 \cdot 255^2$ in our experiments. Fig. 2(e) illustrates the final result after gradient-based improvement.

From Fig. 2(d), we can see certain surrounding tissues that are not part of the prostate are segmented as the prostate. Fig. 3(a) shows prostate region obtained by shape-based level set method, and Fig. 3(b) shows the positive part of the gradient map along y direction: $G_y^+(x, y)$ of DWI image. In Fig. 3(c), the lower smaller component of (b) corresponding to rectum tissues is shown. By extracting (c) from (a), we obtain Fig. 3(d). We apply morphological erosion to (d) and the largest component corresponding to the prostate is shown in Fig. 3(e). The result after morphological dilation is illustrated in Fig. 2(e). We can see that the prostate boundary is restored and the holes in the prostate region are removed.

In Fig. 4, the first row shows the segmentation result by the proposed method, the second row illustrates the ground truth outlined by an expert radiologist, and the third row provides a comparison between our result and ground truth. We observe that our segmentation result is sufficiently close to the result provided by a radiologist.

In addition to visual evaluation, we use dice measure (DSC) to quantitatively evaluate the segmentation result. The DSC is defined as:

$$DSC(A, B) = \frac{2 \cdot |A \cap B|}{|A| + |B|}, \quad (11)$$

where A is the segmentation result, B is the ground truth provided by an expert radiologist, and $|\cdot|$ denotes the number of pixels contained in a set. Table I shows the DSC values for different patients' result obtained by our method.

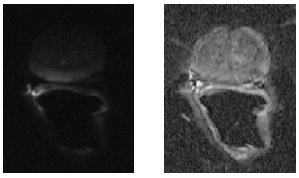

(a) (b)

Fig. 1. Original MR images: (a) DWI image, (b) ADC image.

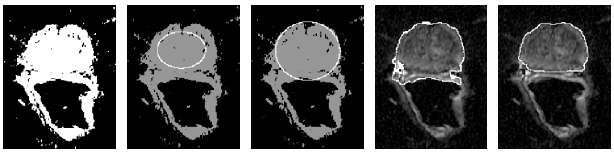

(a) (b) (c) (d) (e)

Fig. 2. (a) ADC image after thresholding, (b) the initial deformable ellipse, (c) the prostate shape is roughly fitted by deformable ellipse, (d) segmentation result of shape-based level set, (e) final result after gradient-based improvement.

IV. Conclusion

Accurate segmentation of prostate from MR images is a crucial step in automated prostate cancer localization. In this paper, we present an unsupervised and fully automatic method to segment prostate gland from MR's ADC and DWI images with a shape-based level set framework. The main contribution of our paper is twofold: (i) we propose to find the shape model of the prostate for a given subject without training; (ii) we propose to use gradient-based methods and morphological operators for more accurate segmentation.

Considering the general prostate shape is elliptical, we first apply deformable elliptical model to fit the prostate region. The obtained deformable ellipse fitting the prostate is then used to initialize and constrain level set evolution with a penalty term. Due to the close proximity of the prostate and rectum, the DWI image's gradient map along y direction is used to remove the tissues of rectum, and morphological operations are applied to smooth the boundary. Our experimental results show that our fully automatic unsupervised method could successfully segment the prostate as can be seen in Table I and Fig. 4.

Future work includes extending our method to 3D MR datasets, applying our method to a larger number of MR dataset and a more in depth analysis of the proposed method.

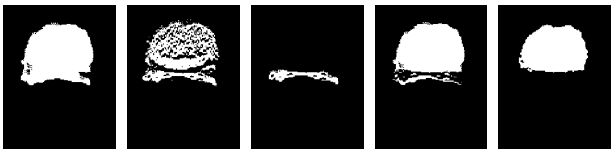

(a) (b) (c) (d) (e)

Fig. 3. (a) Segmentation result after shape-based level set method, (b) the positive part of gradient map of prostate region in DWI image, (c) the lower smaller component of (b), (d) the result obtained by extracting (c) from (a), (e) the largest component of eroded (d).

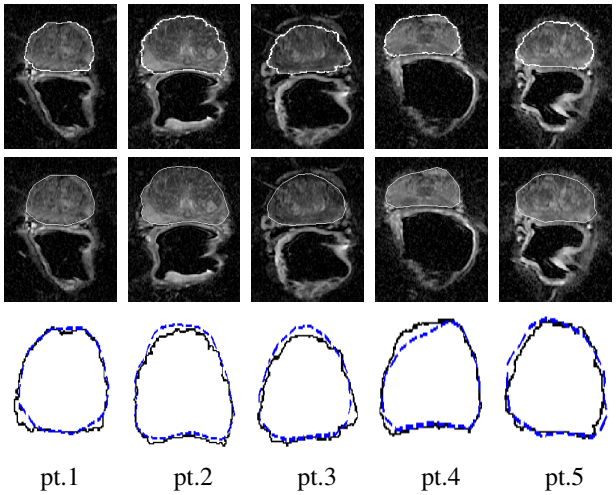

pt.1 pt.2 pt.3 pt.4 pt.5

Fig. 4. Comparison of manual (first row) and automated (second row) segmentation results for five subjects. The third row shows the outlines: manual (dash line) and automated (solid line).

References

[1] American Cancer Society: Cancer Facts and Figures 2007. Atlanta, GA: American Cancer Society, 2007.

[2] J. C. Weinreb and F. V. Coakley, "MR Imaging and MR Spectroscopic Imaging of Prostate Cancer Prior to Radical Prostatectomy: a Prospective Multi-Institutional Clinicopathological Study," presented at *RSNA,* Chicago, IL, 2006.

[3] H. B. Cater, J. Sauvageot, et al. "Prospective Evaluation of Men with Stage T1C Adenocarcinoma of the Prostate," *Journal of Urology,* vol. 157, pp. 2206-2209, 1997.

[4] L. Gong, S. D. Pathak, D. R. Haynor, et al. "Parametric Shape Modeling Using deformable Superellipses for Prostate Segmentation," *IEEE Trans. on Medical Imaging,* vol. 23, pp. 340-349, 2004.

[5] N. N. Kachouie, P. Fieguth, and S. Rahnamayan, "An Elliptical Level Set Method for Automatic TRUS Prostate Image Segmentation," *IEEE International Symposium on Signal Processing and Information Technology,* pp. 191-196, 2006.

[6] A. Tsai, A. Yezzi, W. Wells, et al. "A Shape-Based Approach to the Segmentation of Medical Imagery Using Level Sets," *IEEE Trans. on Medical Imaging,* vol. 22, pp. 137-154, 2003.

[7] M. Samiee, G. Thomas, and R. Fazel-Rezai, "Semi-Automatic Prostate Segmentation of MR Images Based on Flow Orientation," *IEEE International Symposium on Signal Processing and Information Technology,* pp. 203-207, 2006.

[8] N. Otsu, "A Threshold Selection Method from Gray-Level Histograms," *IEEE Trans. on Systems, Man, and Cybernetics,* vol. 9, pp. 62-66, 1979.

[9] S. Osher and J. A, Sethin "Fronts propagating with curvature-dependent speeding: Algorithms based on Hamilton-Jacobi formulation," *Journal of Computational Physics,* vol. 79, pp. 12-49, 1988.

[10] T. Chan and L. Vese, "Active Contours without edges," *IEEE Trans. on Image Processing,* vol. 10, pp. 266-277, 2001.

[11] D. Cremers, N. Sochen and C. Schnorr, "Towards recognition-based variational segmentation using shape priors and dynamic labeling," *In L. Griffith, editor, Int. Conf. on Scale Space Theories in Computer Vision,* vol, 2695 pp. 388-400, 2003.

[12] T. Chan and W. Zhu, "Level Set Based Shape Prior Segmentation," *IEEE Trans. on Image Processing,* vol. 11, pp. 130-141, 2000.

[13] T. F. Chan, B. Y. Sandberg, and L. A. Vese, "Active Contours without Edges for Vector-Valued Images," *Journal of Visual Communication and Image Representation,* vol. 10, pp. 266-277, 2001.